Eur. Phys. J. D **24**, 131–136 (2003)
DOI: 10.1140/epjd/e2003-00103-0

THE EUROPEAN PHYSICAL JOURNAL D

Energetics and dynamics of decaying cluster ions

K. Głuch[1], J. Fedor[1,2], S. Matt-Leubner[1], R. Parajuli[1], C. Mair[1], A. Stamatovic[3], O. Echt[4], C. Lifshitz[5], J. Harvey[6], F. Hagelberg[7], Z. Herman[8], M. Probst[1], P. Scheier[1], and T.D. Märk[1,a]

[1] Institut für Ionenphysik, Leopold-Franzens Universität, Technikerstr. 25, 6020 Innsbruck, Austria
[2] Dept. Plasma Physics, Comenius University, Mlynska Dolina, 84248 Bratislava, Slovak Republic
[3] Faculty of Physics, P.O. Box 368, 11001 Beograd, Yugoslavia
[4] Depart. Physics, University of New Hampshire, Durham, NH 03824, USA
[5] Depart. Physical Chemistry, The Hebrew University of Jerusalem, Jerusalem 91904, Israel
[6] School of Chemistry, University of Bristol, Cantock's Close, Bristol BS8 1TS, UK
[7] Dept. of Physics, Jackson State University, Jackson, MS 39217, USA
[8] J. Heyrovsky Inst. Physical Chemistry, Acad. Sciences, Dolejskova 3, 182 23 Prague 8, Czech Republic

Received 10 September 2002
Published online 3 July 2003 –

Abstract. The recent addition of (i) a third sector field to our two sector field mass spectrometer (resulting in a BE1E2 field configuration) and of (ii) a high performance electron gun enables us now to study in detail the time dependence of the kinetic energy release distribution (KERD) over a relatively wide range of cluster ion lifetimes. Using this newly constructed device we have studied here for the first time KERDs and deduced binding energies BEs (using finite heat bath theory) of large rare gas cluster ions (an upper size limit in earlier studies arose from the fact that different naturally occurring isotopes will contribute to a chosen metastable peak when the size exceeds a certain value) and in addition of fullerene ions smaller and larger than C_{60}^+ (here again contaminating coincidences did not allow such studies earlier). Moreover, high precision KERD measurements for the decay of rare gas dimer ions in conjunction with model calculations (using recently calculated potential energy curves for the rare gas dimer ions) also enable us to obtain information on the dynamics and the mechanisms of the underlying spontaneous decay reactions $Rg_2^{+*} \rightarrow Rg^+ + Rg$. In addition, we are also reporting here a novel method (unified breakdown graph method) to determine cluster ion binding energies using a recently constructed tandem mass spectrometer BESTOF allowing us to measure fragmentation patterns arising from the unimolecular decay of molecular cluster ions induced by surface collisions. The fragmentation and reaction patterns of protonated ethanol cluster ions investigated here clearly demonstrate in contrast to some of the earlier cluster ion studies that unimolecular dissociation kinetics determines the formation of product ions in the surface-induced decomposition.

PACS. 36.40.Qv Stability and fragmentation of clusters – 36.40.Wa Charged clusters

1 Introduction

Fragmentation of finite size systems is a widely spread phenomenon in nature, including such diverse phenomena as the break-up of sub-microscopic objects or collisions between asteroids [1,2]. The study of fragmentation of systems like nuclei, molecules and clusters has attracted much interest recently and one intriguing result is the recognition that some of the general features of this phenomenon (*e.g.* fragmentation patterns) are rather independent of the actual system studied and its corresponding interaction forces [3]. It is well-known that highly excited finite atomic systems will relax by either emitting electrons, neutral particles (dissociation), or a continuous spectrum of photons. These reactions are the molecular analogues to thermionic electron emission, evaporation, and black body radiation in solid state physics. Moreover, multiply charged systems may decay *via* fission reactions ejecting charged rather than neutral fragments analogous to nuclear fission [4]. It is thus not surprising that one important field in cluster science (attracting recently growing interest [3–5]) is the study of the fragmentation behaviour of excited cluster ions, X_n^{z+*}

$$X_n^{z_1+*} \rightarrow \sum X_p^{z_2+}, \quad z_2 \leq z_1 \tag{1}$$

[a] e-mail: tilmann.maerk@uibk.ac.at
also adjunct professor at Dept. Plasma Physics, Comenius University, 84248 Bratislava, Slovak Republic.

produced by such means as photon, electron and ion impact (including charge transfer reactions), collision induced dissociation (CID) reactions or surface collisions.

Mass spectrometric studies of spontaneous (metastable) decay reactions and of (prompt) dissociative reactions of mass-selected cluster ions induced by photons, electrons, heavy particles (CID) or surface collisions have provided a wealth of information about structure, stability and energetics of these species and the dynamics of the corresponding decay reactions [5]. Surprisingly few studies, however, have been reported concerning measurements of the kinetic energy release distribution (KERD) for the decay of such excited cluster ions. The most common mechanism that drives the unimolecular, metastable decay of atomic cluster ions is vibrational predissociation in which the excess energy is statistically distributed over all energetically accessible degrees of freedom. Metastable cluster ions observed at time t after excitation will therefore contain a maximum amount of excess energy E^* that is given by the condition that their decay rate constant $k(E^*)$ cannot exceed $1/t$. The number of monomers that can be evaporated sequentially [6] in a mass spectrometer within a typical observational time window of duration $\Delta t \leq t$ (*e.g.* 10 to 100 μs) rarely exceeds one, and never two, because evaporation will reduce E^* and lead to a dramatic reduction in the rate constant for loss of the next monomer unless the cluster contains hundreds of atoms [7].

However, unimolecular dissociation may also be driven by mechanisms that involve non-statistical, localized storage of excess energy. For example, large amounts of energy can be stored in nitrogen cluster ions in form of intramolecular vibrations [8]; other examples involve delayed isomerization reactions in molecular cluster ions [9], or charge transfer between doubly charged atoms and neutral molecules in a cluster [10]. Another mechanism involves electronically excited states in rare gas cluster ions: one characteristic feature of this exciton-driven decay is the large amount of energy that is abruptly released within the metastable time window [11].

2 Experimental

Using a high resolution two sector field mass spectrometer of reversed geometry (BE) we have measured in the past years metastable fractions and mass-analyzed ion kinetic energy (MIKE) peaks for metastable (spontaneous) and electron-induced decay reactions involving monomer evaporation and fission reactions of atomic and molecular cluster and fullerene ions. Both, average kinetic energy release, $\langle KER \rangle$, data derived from the peak shapes and the time dependence of the metastable fractions show a characteristic dependence on cluster size yielding immediate information on the metastable fragmentation mechanism when going for instance from the oxygen dimer to the decamer ion [12]. Moreover, the $\langle KER \rangle$ data contain information about the transition state temperature and thus

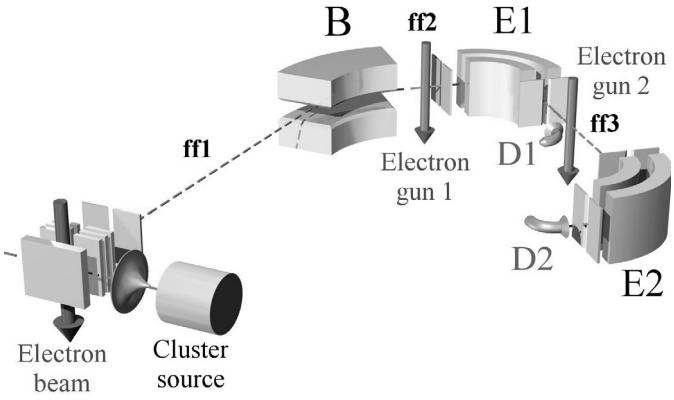

Fig. 1. Three sector field mass spectrometer.

one can use finite heat bath theory to calculate the binding energies of the decaying cluster ions allowing on the one side for rare gas [13] and molecular [14] cluster ions informative comparison with (i) previous results based on gas phase ion equilibria measurements where available and with (ii) the corresponding bulk value and on the other side the final solution of the longstanding C_{60} binding energy (BE) problem (see a summary and references in [15]).

The recent addition of (i) a third sector field to this two sector machine (resulting in a BE1E2 field configuration), see Figure 1 and of (ii) a high performance electron gun enables us now to also study in detail the time dependence of the kinetic energy release distribution (KERD) over a relatively wide range of ion lifetimes (see a first application involving a combined experimental and theoretical study of the time-resolved average kinetic energy release $\langle KER \rangle$ of the $H^{\cdot}$ loss reaction in propane leading to the *sec*-propyl cation, $C_3H_8{}^+ \rightarrow$ *sec*-$C_3H_7^+ + H^{\cdot}$ [16]). Moreover, high precision KERD measurements for the decay of rare gas dimer ions in conjunction with model calculations (using recently calculated potential energy curves for the rare gas dimer ions of Ne, Ar, Kr and Xe) also enable us to obtain information on the dynamics and the mechanisms of the underlying spontaneous decay reactions $Rg_2^+ \rightarrow Rg^+ + Rg$, *i.e.* leading to the conclusions that these metastable dissociations are not due to the well-known mechanisms for small molecular ions such as electronic predissociation and/or due to tunneling, but are of the exotic type where dipole allowed spontaneous radiative decay initiates the molecular dissociations.

Moreover, the use of a second electrostatic analyzer E2 has additional advantages as described by Beynon and coworkers [17]. First of all, in a "normal" MIKE spectrum recorded in ff2, the decay of fragment ions m_2 produced in ff1 from precursor ions m_1 with $m_1 > m_p$ will also contribute to the MIKE spectrum if their apparent mass $m^* = m_2^2/m_1$ is approximately equal to the decaying parent ion mass m_p; this problem is the more serious the larger the cluster ions under study. In contrast MIKE spectra recorded in ff3 are free of these artifact peaks because those fragment ions will not pass through E1 (see

a first application determining the kinetic energy release in Coulomb explosion of metastable $C_3H_5^{2+}$ decaying into $C_2H_2^+ + CH_3^+$ [18]). Another advantage is the possibility to analyze decay reactions occurring in ff2 by simultaneously scanning E1 and E2. In this "linked scan" mode the energy resolution is enhanced without losing much of the sensitivity, *i.e.*, closing the exit slit behind E1 as much as possible while using an open collector slit behind E2. We have tested our BE1E2 system by measuring metastable H loss from $C_3H_8^{+\cdot}$ with this linked scan technique, and obtained a $\langle KER \rangle = 8.33 \pm 0.67$ meV. Our previous result for this reaction, using a normal MIKE scan [19], was $\langle KER \rangle = 9.3 \pm 1.5$ meV which agrees quite well within the experimental uncertainty.

Using this newly constructed device we have studied here for the first time KERDs and BEs of large rare gas cluster ions (an upper size limit in earlier studies arose from the fact that different naturally occurring isotopes will contribute to a chosen metastable peak when n exceeds a value, *e.g.* for neon above $n = 13$) and in addition of fullerene ions smaller and larger than C_{60}.

In addition, we are also reporting here a novel method to determine cluster ion binding energies using a recently constructed tandem mass spectrometer BESTOF [20] allowing us to measure fragmentation patterns arising from the unimolecular decay of molecular cluster ions induced by surface collisions. This BESTOF apparatus (see Fig. 2) consists of a double focusing two-sector-field mass spectrometer in reversed geometry (BE) combined with a surface (S) collision chamber and a linear time-of flight (TOF) mass spectrometer. Neutral clusters are produced by supersonic expansion through a 20 μm nozzle in a continuous cluster source. In the present experiments (see also previous experiments on benzene clusters [21], acetone clusters [22,23] and acetonitrile clusters [24]) neutral ethanol cluster beams are prepared by supersonic expansion of a helium/ethanol gas mixture at the pressure of the seeding gas (He) of 1.5 bar and at a stagnation temperature in the expansion vessel of about 300 K. After passing through a skimmer, the neutral beam enters transversely into a Nier-type electron impact ion source. Neutral clusters are ionized in this ion source by the impact of 80 eV electrons. The ions produced are extracted from the ion source region and accelerated to 3 keV for mass (and energy) analysis by the double-focusing two-sector-field mass spectrometer. The nominal mass resolution of this mass spectrometer can be at 3 keV acceleration as high as 10 000. However, in this work the slits were completely opened and the resolution was about 150. After passing the mass spectrometer exit slit, the ions are refocused by an Einzel lens and decelerated to the required collision energy before interacting with the target surface. Field penetration effects are minimized by shielding the target with conical shield plates. The incident impact angle of the projectile ions is kept at 45° and the scattering angle (defined as a deflection from the incident beam direction) is fixed at 91°. The collision energy of ions impacting on the surface is defined by the potential difference between the ion source and the surface. The potential difference

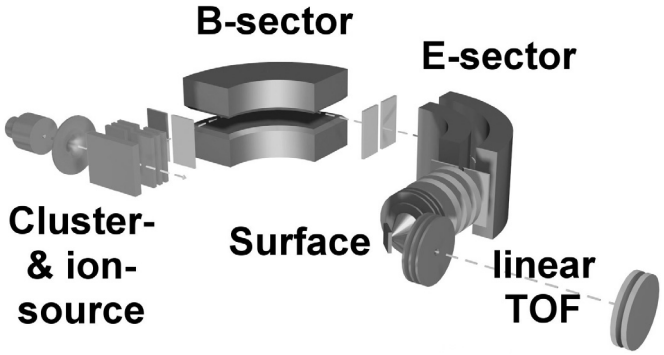

Fig. 2. BESTOF apparatus.

(hence, the collision energy) can be varied from about zero to 2 keV with a typical resolution of about 200 meV (full width at half maximum). The collision energy and a measure of the projectile beam energy spread is determined by applying to the target a retarding potential and measuring the (reflected) total ion signal as a function of the target potential. A fraction of the product ions formed at the surface leaves the shielded chamber through a 1 mm diameter orifice. The ions are then subjected to a pulsed extraction-and-acceleration field that initiates the time-of-flight analysis of the ions. The second mass analyzer is a linear time-of-flight mass selector with a flight tube of about 80 cm length. The mass selected ions are detected by a double-stage multi-channel-plate connected to a fast scaler (time resolution of 5 ns per channel) and a laboratory computer. The surface used here, similarly as in our earlier experiments, consists of a polished stainless steel surface maintained under ultra high vacuum conditions (10^{-9} torr) in our bakeable turbo-pump evacuated target collision chamber. However, even these conditions do not exclude deposition of hydrocarbons on the surface, whenever the valve between the mass spectrometer and the target collision chamber was opened and the pressure in the target region increased to about $5 - 8 \times 10^{-9}$ torr.

3 Results

3.1 Binding energy of large rare gas cluster ions

As mentioned above, we were not able in earlier studies to extend KERD and BE measurements for rare gas cluster ions above a certain size due to interferences from isotopomers. The present three sector field set-up allows the measurement of the corresponding KERDs without any ambiguity and BEs derived using finite heat bath theory are given in Figure 3 in comparison to other data. It can be clearly seen that in contrast to our earlier measurements [13] using the two sector field apparatus where BE data did increase due to interference from isotopomers above a certain size (these artifact data are not shown in the figure), the present data (designated full squares) appear to extend smoothly the earlier data to higher n and tend as expected to approach the bulk value.

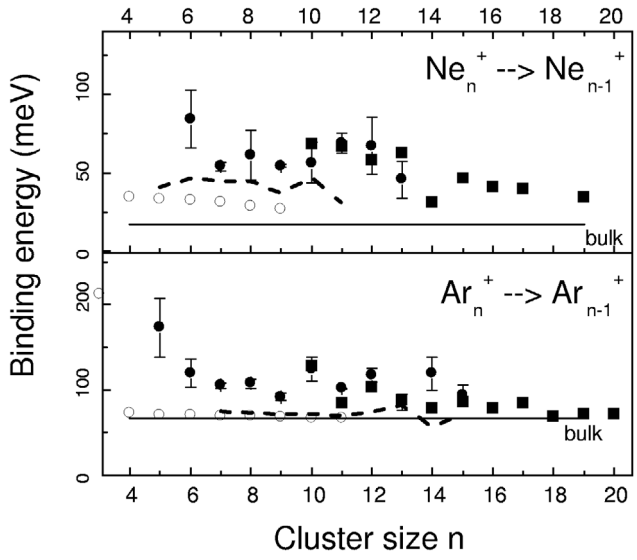

Fig. 3. Binding energies of Ne and Ar cluster ions calculated from the average $\langle KER \rangle$ with finite heat bath theory and a constant Gspann factor of $\gamma = 23.5$ (full dots: earlier measurements with two sector field apparatus [13], full squares: present measurements with three sector field apparatus). Open circles: results from high-pressure gas phase experiments [25]. Full horizontal line: enthalpy of vaporization of the bulk [26]. Dashed line: Binding energy calculated theoretically for Ne_n^+ [27] and Ar_n^+ [28].

3.2 Binding energy of fullerene ions

As mentioned above the dissociation energy for C_2 emission from the C_{60}^+ cation has been recently ascertained to be 10.0 ± 0.2 eV, the reason for the earlier scatter of data being the fact that the transition state of the metastable C_{60}^+ ion has rather unusual properties leading to a Gspann factor of 33.8 instead of the generally accepted value of 23 to 25 (for details on the definition of the Gspann factor see Ref. [15]). One still unsolved question, however, remained, namely whether C_{60}^+ is sitting on the leading edge of a magic shell (as originally proposed by Klots [29] and discussed by Lifshitz [30]) or whether the dissociation energy as a function of n has a single very high value at $n = 60$ corresponding to a magic number model (supported by relative BEs measured by Barran *et al.* [31] and recent absolute measurements of Tomita *et al.* [32]). In order to solve this open point we have measured here in an unambiguous way (see discussion above) KERDs of fullerene ions below and above C_{60}^+ and derived the corresponding binding energies (for details of the method see papers mentioned above). The preliminary results given in Figure 4 confirm the occurrence of a magic shell around size 60 rather than the model of magic numbers, *i.e.*, the binding energy values are increasing without exception from 52 to 60, then at the beginning of the next shell there is a strong drop from 60 to 62 and then starts again a continuous increase of the BE. It is interesting to note that in principle there is a good agreement between the three data sets, the only important exception (besides the fact that the data of Tomita *et al.* are lower for 62 to 68) is size 58 where both earlier data sets are lower and indicate a drop of the binding energy when going from 56 to 58.

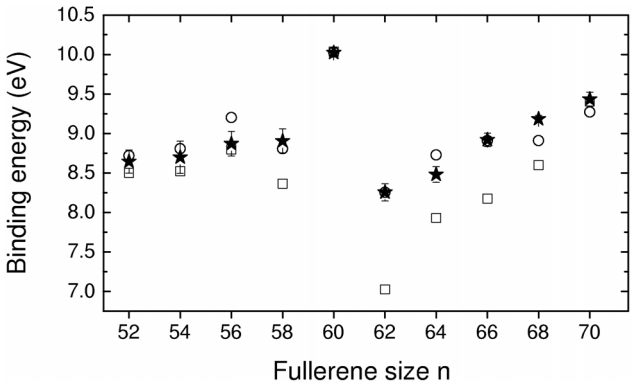

Fig. 4. Dissociation energy of fullerene cations C_n^+ as a function of cluster size n. Stars with standard deviation error bars: present results, open squares: results of Tomita *et al.* [32], open circles: results of Barran *et al.* [31]. In order to allow a better comparison between the three data sets the two earlier data sets have been normalized to the present C_{60}^+ value.

3.3 Binding energy of protonated ethanol cluster ions

Using our recently constructed tandem mass spectrometer system BESTOF (consisting of a double focusing two-sector-field mass spectrometer in reversed geometry (BE) combined with a surface (S) collision chamber and a linear time-of flight (TOF) mass spectrometer) we have carried out systematic investigations (using also deuterated molecules) on the interaction of protonated ethanol cluster ions (the major ions being produced in the primary electron impact ionization spectra of neutral ethanol clusters [33]) with a hydrocarbon covered stainless steel surface. The results obtained here show for the first time clear evidence that unimolecular dissociation kinetics determines the production of the observed decay patterns in collision energy resolved mass spectra (CERMS are spectra where the relative abundances of all product ions are plotted as a function of the collision energy). If CERMS curves of the protonated ethanol trimer $(C_2H_5OH)_3H^+$, dimer $(C_2H_5OH)_2H^+$, and monomer $(C_2H_5OH)H^+$ ion, as obtained from the series of secondary mass spectra measured at a series of collision energies, are plotted above each other, one sees that shifting these three plots along the energy axis against each other results in a situation where certain characteristic features, *i.e.*, crossings of the major product ion abundances, occur at the same energy axis position. For instance, in order to reach an overlap for the crossing between the product ion $(C_2H_5OH)H^+$ and $C_2H_5^+$ the CERMS plots of the protonated dimer $(C_2H_5OH)_2H^+$ with respect to the protonated trimer needs to be shifted by 16 eV, in order to reach an overlap for the crossing between the product ion $(C_2H_5OH)H^+$ and $C_2H_3^+$ the CERMS plots of the protonated monomer with respect to the trimer curve needs to be shifted by about 43 eV and with respect to the dimer by about 27 eV.

The shifts of the collision energy scale for the three projectiles evidently indicate energy differences required to achieve the same degree of fragmentation in the projectile and thus they should be related to the binding energy of the evaporating monomer molecule to the respective cluster ion. Assuming the collisional-to-internal energy transfer for this type of surface to be about 6% (see recent experiments on energy transfer in surface collisions [34,35]), we can derive from the shifts of the energy scale a value of the dissociation energy of an ethanol molecule from the protonated ethanol trimer $D[(C_2H_5OH)_2H^+ - C_2H_5OH] = 0.06 \times (41-25) = 0.95$ eV, and for the protonated dimer $D[(C_2H_5OH)H^+ - C_2H_5OH] = 0.06 \times (45-18) = 1.6$ eV. It is interesting to note that these values are of the same order of magnitude as calculated binding energies for the corresponding ions, *i.e.*, of 0.92 eV for the trimer and 1.38 eV for the dimer ion [36].

As mentioned above there is an obvious similarity in the CERMS patterns if shifted in the way as described. However, the patterns seem to be more and more compressed when going from the protonated trimer to the protonated monomer. The compression of the CERMS curve pattern when going from the protonated trimer projectile to the protonated monomer is due to the fact that for different projectiles the same energy is distributed over a different number of internal degrees of freedom. A unification of the picture can be achieved by normalizing the energy scale to the energy pertinent to a single degree of freedom. For a system behaving like a statistical ensemble, the number of internal degrees of freedom is $idf = (3N - 6)$, where N is the number of atoms in the system. For the protonated trimer ($N_3 = 28$), dimer ($N_2 = 19$) and monomer ($N_1 = 10$) these *idf* numbers are 78, 51, and 24, respectively. The relation between the energy pertinent to one internal degree of freedom and the collision energy is then $\langle E_{int}\rangle_{idf} = 0.06E_{coll}/(3N_i - 6)$. The corresponding unified CERMS curves are shown as a function of this new energy scale in Figure 5. The mutual overlap of data from surface collisions of three different projectiles, the protonated trimer, dimer and monomer, is remarkably good. We thus obtain a unimolecular decomposition pattern of the protonated trimer over a wide range of energies by a combination of data from experiments on surface-induced dissociation of the three different projectiles. The internal energy of the trimer is then simply $\langle E_{int}\rangle_3 = (3N_3 - 6)\langle E_{int}\rangle_{idf} = 78\langle E_{int}\rangle_{idf}$ (upper scale in Fig. 5) and covers values up to about 9.8 eV. Recent experiments clearly show that the energy transformed in a surface collision to internal energy of a polyatomic projectile increases linearly with the collision energy and the width of its distribution does not change much with the collision energy. Thus in a surface collision a certain specific internal energy can be imparted to the projectile. It appears that surface collision excitation may possibly be used to obtain information on the break-down pattern of an excited polyatomic ion in an analogous way as charge transfer was used many years ago (see, *e.g.* Refs. [37,38]). The necessary requirement, however, is that the width of imparted energy distribution should not be too wide

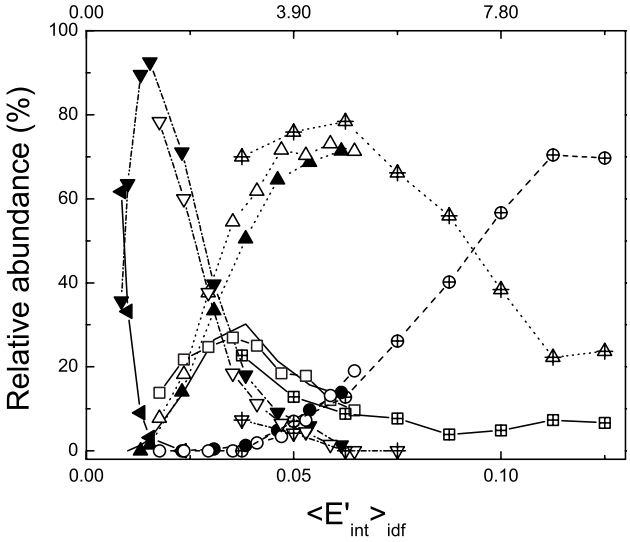

Fig. 5. Unified break-down graph for the protonated ethanol cluster ions $(C_2H_5OH)_nH^+$ up to $n = 3$. Dependencies of the relative abundance of product ions on the internal energy per internal degree of freedom $\langle E'_{int}\rangle_{idf}$ as obtained from corresponding CERMS of $(C_2H_5OH)_3H^+$ (full symbols), $(C_2H_5OH)_2H^+$ (open symbols), and $(C_2H_5OH)H^+$ (symbols with cross inside) for the fragment ions H_3O^+ (squares), $C_2H_3^+$ (circles), $C_2H_5^+$ (triangles), $(C_2H_5OH)H^+$ (inverted triangles), $(C_2H_5OH)_2H^+$ (triangles pointing to the left). Upper scale shows the internal energy of the trimer ion in eV.

in comparison with the changes of relative abundance of fragment ions in the break-down pattern. A typical energy distribution imparted to a polyatomic projectile in a surface collision, as derived from recent data for this type of surface, has a full width half maximum of about 1.5 eV. The situation is not ideal, but the data suggest that the recalculated CERMS curves in Figure 5 may be regarded as a relevant break-down pattern of the protonated ethanol trimer ion. It is interesting to note that the present method to determine binding energies (for more details see [39]) is reminiscent of the so-called model free approach presented at the same ISSPIC conference as the present contributions, see reference [40].

Work supported by FWF, ÖNB, ÖAW, Wien and the European Commission, Brussels.

References

1. H. Hutchinson, Science **80**, 693 (1998)
2. R.P. Binzel, Nature **88**, 516 (1997)
3. E. Pfefferkorn, *Fragmentation Phenomena*, edited by D. Beyson, X. Campi, (World Scientific, Singapure 1995)
4. O. Echt, T.D. Märk, in *Clusters of Atoms and Molecules II*, edited by H. Haberland (Springer-Verlag, Heidelberg 1994), p. 183
5. T.D. Märk, O. Echt, in *Clusters of Atoms and Molecules II*, edited by H. Haberland (Springer-Verlag, Berlin 1994), p. 154
6. P. Scheier, T.D. Märk, Phys. Rev. Lett. **59**, 1813 (1987)

7. C.E. Klots, J. Phys. Chem. **92**, 5864 (1988)
8. P. Scheier, T.D. Märk, Chem. Phys. Lett. **148**, 393 (1988)
9. M. Foltin, V. Grill, T. Rauth, Z. Herman, T.D. Märk, Phys. Rev. Lett. **68**, 2019 (1992)
10. C.A. Woodward, M.P. Dobson, A.J. Stace, J. Phys. Chem. **100**, 2279 (1997)
11. O. Echt, R. Parajuli, S. Matt, A. Stamatovic, P. Scheier, T.D. Märk, Chem. Phys. Lett. **361**, 91 (2002)
12. S. Matt, R. Parajuli, A. Stamatovic, P. Scheier, T.D. Märk, J. Chem. Phys. **116**, 7583 (2002)
13. R. Parajuli, S. Matt, O. Echt, A. Stamatovic, P. Scheier, T.D. Märk, Chem. Phys. Lett. **352**, 288 (2002)
14. R. Parajuli, S. Matt, A. Stamatovic, T.D. Märk, P. Scheier, Int. J. Mass Spectr. **220**, 221 (2002)
15. S. Matt, O. Echt, P. Scheier, T.D. Märk, Chem. Phys. Lett **348**, 194 (2001)
16. S. Matt-Leubner, A. Stamatovic, R. Parajuli, P. Scheier, T.D. Märk, O. Echt, C. Lifshitz, Int. J. Mass Spectr. **222**, 213 (2003)
17. M. Guilhaus, R.K. Boyd, A.G. Brenton, J.H. Beynon, Int. J. Mass Spectrom. Ion Proc. **67**, 209 (1985)
18. K. Gluch, J. Fedor, S. Matt-Leubner, O. Echt, A. Stamatovic, M. Probst, P. Scheier, T.D. Märk, J. Chem. Phys. (in print, 2003)
19. S. Matt, O. Echt, A. Stamatovic, T.D. Märk, J. Chem. Phys. **113**, 616 (2000)
20. C. Mair, T. Fiegele, F. Biasioli, R. Wörgötter, V. Grill, M. Lezius, T.D. Märk, Plasma Sources Sci. Technol. **8**, 191 (1999)
21. R. Wörgötter, C. Mair, T. Fiegele, V. Grill, T.D. Märk, H.Schwarz, Int. J. Mass Spectr. Ion Proc. **164**, L1 (1997)
22. C. Mair, T. Fiegele, F. Biasioli, J.H. Futrell, Z. Herman, T.D. Märk , Int. J. Mass Spectrom. Ion. Proc. **188**, L1-L6 (1999)
23. C. Mair, T. Fiegele, F. Biasioli, Z. Herman, T.D. Märk, J. Chem. Phys. **111**, 2770 (1999)
24. C. Mair, Z. Herman, J. Fedor, M. Lezius, T.D.Märk, J. Chem. Phys. (in print, 2003)
25. K. Hiraoka, T. Mori, J. Chem. Phys. **90**, 7143 (1989)
26. D.R. Lide, *CRC Handbook of Chemistry and Physics* (CRC Press, Boca Raton, 2000)
27. F. Sebastianelli, E. Yurtsever, F.A. Gianturco, Int. J. Mass Spectrom **220**, 193 (2002)
28. H.U. Böhmer, S.D. Peyerimhoff, Z. Phys. D **11**, 239 (1989)
29. C.E. Klots, Z. Phys. D **21**, 335 (1991)
30. C. Lifshitz, Int. J. Mass Spectrom. **198**, 1 (2000)
31. P.E. Barran, S. Firth, A.J. Stace, H.W. Kroto, K. Hansen, E.E.B. Campbell, Int. J. Mass Spectrom. Ion Proc. **167**, 127 (1997)
32. S. Tomita, J.U. Anderson, C. Gottrup, P. Hvelplund, U.V. Pedersen, Phys. Rev. Lett. **87**, 073401 (2001)
33. W.Y. Feng, C. Lifshitz, Int. J. Mass Spectrom. Ion Proc. **149/150**, 13 (1995)
34. J. Kubista, Z. Dolejsek, Z. Herman, Eur. Mass Spectrom. **4**, 311 (1998)
35. F. Biasioli, T. Fiegele, C. Mair, Z. Herman, O. Echt, F. Aumayr, H.-P. Winter, T.D. Märk, J. Chem. Phys. **113**, 5503 (2000)
36. V.M. Jarvis, M.A. Villanueva, D.E. Bostwick, T.D. Moran, Org. Mass Spectrom. **28**, 595 (1993)
37. V. Cermak, Z. Herman, Nucleonics **19**, 106 (1961)
38. E. Lindholm, in *Ion-Molecule Reactions*, edited by J.L. Franklin (Plenum, New York 1972), Vol. 2, p. 457
39. C. Mair, J. Fedor, M. Lezius, P. Scheier, M. Probst, Z. Herman, T.D. Märk, New J. Phys. **5**, 91 (2003)
40. L. Schweikhard, K. Hansen, A. Herlet, G. Marx, M. Vogel, Eur. Phys. J. D **24**, 137 (2003)